ORIGINAL RESEARCH **Open access**

Effects of Wind Speed and Nozzle Type on Spray Deposition and Drift from a Remotely Piloted Aerial Application System

Sofía Martínez[1*], Carlos Gómez[1]

Abstract

The extraordinary expansion of remotely piloted aerial application systems (RPAASs) over recent years has prompted scrutiny of their impact on off-target displacement of crop protection agents. The spray droplet spectrum is a principal governing factor that dictates droplet pathways and off-target transport of pesticide particulates. A field experiment was executed to contrast in-swath and downwind spray accumulation on terrestrial collectors from a 20 L RPAAS unit, outfitted with three distinct nozzles supplying fine, medium, and extra-coarse droplet distributions. A fluorescent tracer was employed to ascertain spray deposition. Suspended spray droplets were captured at distances of 10 and 20 m downwind. Downwind accumulation on ground collectors showed that the extra-coarse nozzle accumulated markedly lower deposits than either the medium or fine nozzle. Correspondingly, airborne deposition originating from the extra-coarse nozzle was substantially diminished when measured against the fine or medium nozzle. Linear mixed-effects modeling substantiated these outcomes and revealed that wind velocity acted as a covariate, sharpening the differences in deposition across nozzle types. Findings indicated that spray displacement from RPAAS platforms can be alleviated by selecting appropriate nozzles that generate coarser droplet distributions. These outcomes will equip aerial applicators with deeper insight into optimal management protocols for drift reduction.

Keywords UAV, UAS, RPAAS, Deposition, Spray drift, Spray drone

*Correspondence:
Sofía Martínez
sofia.martinez@upm.es
[1] Department of AI for Olive Orchard Yield and Disease Modeling, Faculty of Agriculture, Polytechnic University of Madrid, Madrid, Spain

Introduction

Unmanned aerial vehicles (UAVs) or remotely piloted aerial (or aircraft) application systems (RPAASs) have surged in prevalence worldwide in recent years, overhauling established agricultural practices with an inventive treatment modality grounded in autonomous aerial spray delivery. Notwithstanding varied market share intelligence reported for the drone sector [1], one analysis anticipated that the present market stands favorably positioned for continued growth, chiefly attributable to governmental backing across multiple nations, economic efficiency, the debut of larger units capable of servicing expansive acreages, and the fusion of precision agriculture with AI technologies designed to overhaul the agricultural domain by furnishing growers with streamlined land and crop oversight frameworks [2]. The valuation of the U.S. agricultural drone market stood at USD 1.39 billion in 2021 and is projected to grow at a compounded annual rate of 35.79% over the near term, with the spray drone segment forecast to reach an overall value of USD 11.9 billion by 2028 [3]. With the amplified manufacture of UAVs, the projected economic gains for the U.S. aerospace sector are expected to quicken employment growth and the generation of supplementary proceeds, surpassing USD 82 billion cumulatively from

This is an open access article distributed under the terms of the Creative Commons Attribution-NonCommercial-ShareAlike 4.0 International License (CC BY-NC-SA 4.0), which permits non-commercial use, distribution, reproduction, and adaptation in any medium or format, provided that appropriate credit is given to the original author(s) and source, a link to the license is provided, and any changes made are indicated. Adapted material must be distributed under the same license.

© 2022 The Author(s). | Published by Agro Intelligence Research Press

2015 to 2025 [3]. Goldman Sachs indicated that current spray-drone capabilities have already outpaced piloted aircraft in endurance, range, operational safety, and cost-effectiveness, and that forthcoming drone generations will incorporate superior stealth, sensing, payload, autonomous operation, and communication capabilities [4].

Parallel to the unprecedented proliferation of UAVs across agricultural operations in the United States and South Asian nations, escalating unease surrounds their suitability for downwind deposition through off-target drift of crop protection substances. While pesticide deployment faces tighter regulatory oversight in the United States than in many other jurisdictions, a growing global expectation exists among producers, applicators, and manufacturers to furnish corroborative evidence to enable the safe delivery of pesticides via this newly emergent, technology-driven spray application modality. Consistent with this need, the OECD, alongside other investigators, assembled an exhaustive synthesis of published research concerning RPAASs to facilitate the evidential requirements indispensable for the safe operation of this technology [5-7]. In pursuit of this collective mission, producing field-derived datasets to evaluate and interpret the performance of crop protection products deployed from RPAAS platforms is essential, thereby providing empirical observations to aid the construction of predictive models characterizing the fate of spray droplets as they are discharged from spray drones. Chen *et al.* [8] explored spray deposition and drift under field conditions, observing that drift magnitude rose in tandem with wind speed, whereas Dv0.5 droplet dimensions shrank, and that Dv0.5 droplets measuring 185 μm displayed enhanced penetration within rice canopies. Wang *et al.* [9] assessed in-swath accumulation and downwind displacement from a quad-rotor drone equipped with centrifugal nozzles across field plots, using three droplet size classes (100, 150, and 200 μm) and varying wind regimes. Wang *et al.* [9] noted that elevating the rotational velocity of the centrifugal nozzle from 2000 rpm to 17,000 rpm shifted the DSC rating from extra-coarse to fine classifications. Working within a turfgrass setting, Koo *et al.* [10] established that for crabgrass suppression, deployment altitude ought to remain minimal, given that aggregate deposition lessened by 6% per meter of added height, plausibly owing to evaporative losses. Wongsuk *et al.* [11] reported that increased flight elevation and finer droplet spectra produced amplified drift readings. At the same time, the inclusion of an adjuvant and utilization of an air-induction nozzle curtailed drift to below 3 m aboveground for a hexa-rotor UAV.

The trajectory behavior of spray droplets discharged from piloted aircraft was mathematically modeled as early as 1979 to forecast operational flight modifications in real time [12]. The RPAAS platform, conversely, exhibits superior agility relative to manned aircraft and can operate safely at substantially lower altitudes under computerized navigational control, thereby creating demand for mathematical instruments that enable instantaneous prediction and modification of spray deposition under these conditions. Further, RPAAS units are marketed in an array of configurations with variable payload volumes, rotor thrust outputs, and power specifications. They are supplied with manufacturer-integrated nozzle assemblies that deliver distinct spray droplet spectra [13].

Although spray-displacement simulations conducted in wind tunnels help understand droplet trajectories under controlled conditions, they fall short of capturing drift phenomena in field settings, where meteorological unpredictability plays a commanding yet decisive role [14]. Tangible advantages sought from this emergent technology across agricultural landscapes can only be realized by understanding the foundational elements that guide effective stewardship and the functioning of RPAASs at every flight pass.

This investigation aimed to quantify the in-swath and downwind disposition of an aerially delivered spray mixture when deployed from an RPAAS unit. The spray droplet spectrum has been thoroughly documented as a pivotal parameter used by aerial applicators to reduce spray drift. Solutions with coarser droplet distributions exhibit diminished horizontal or off-target displacement by virtue of increased mass and shorter settling times on vegetative surfaces. In the present study, Turbo TeeJet air-induction (TTI) nozzles that generate extra-coarse droplets were evaluated against extended-range (XR) and Turbo TeeJet (TT) nozzles that produce fine-to-medium droplets.

Materials and Methods

© 2022 The Author(s). | Published by Agro Intelligence Research Press

The investigation was conducted on an unpaved plot overlain with gravel in Burleson County, near College Station, TX (30°40′ N, 96°18′ W). The RPAAS deployed for the experiment was a V8A Pro (Homeland Surveillance and Electronics, Casselberry, FL, USA) rated for a 20 L payload capacity **(Figure 1)**. The experiment encompassed three treatments, each repeated 20 times. Under treatment 1, the RPAAS was configured with extended range flat-fan spray nozzles, XR 110-01 (Spraying Systems Inc., Wheaton, IL, USA), which yielded fine sprays; treatment 2 employed wide-angle flat-fan spray nozzles, TT 110-01 (Spraying Systems Inc., Wheaton, IL, USA), yielding medium sprays; and treatment 3 utilized extra-coarse sprays produced by air-induction flat-fan spray nozzles, TTI 110-01 (Spraying Systems Inc., Wheaton, IL, USA). The V8A Pro carried four nozzles, positioned two to the right and two to the left of the boom. Nozzles were spaced at distances of 18″ (45.7 cm) and 32″ (81.3 cm) from the aircraft centerline for the inboard and outboard positions, respectively **(Figure 2)**.



Figure 1. The V8A Pro aircraft is rated with a 20 L payload capacity, eight (8) rotors, and four (4) spray nozzles mounted on a boom, as utilized in this experiment. Nozzles were located at 18” (45.7 cm) and 32” (81.3 cm) from the aircraft centerline for the inboard and outboard positions, respectively.

© 2022 The Author(s). | Published by Agro Intelligence Research Press

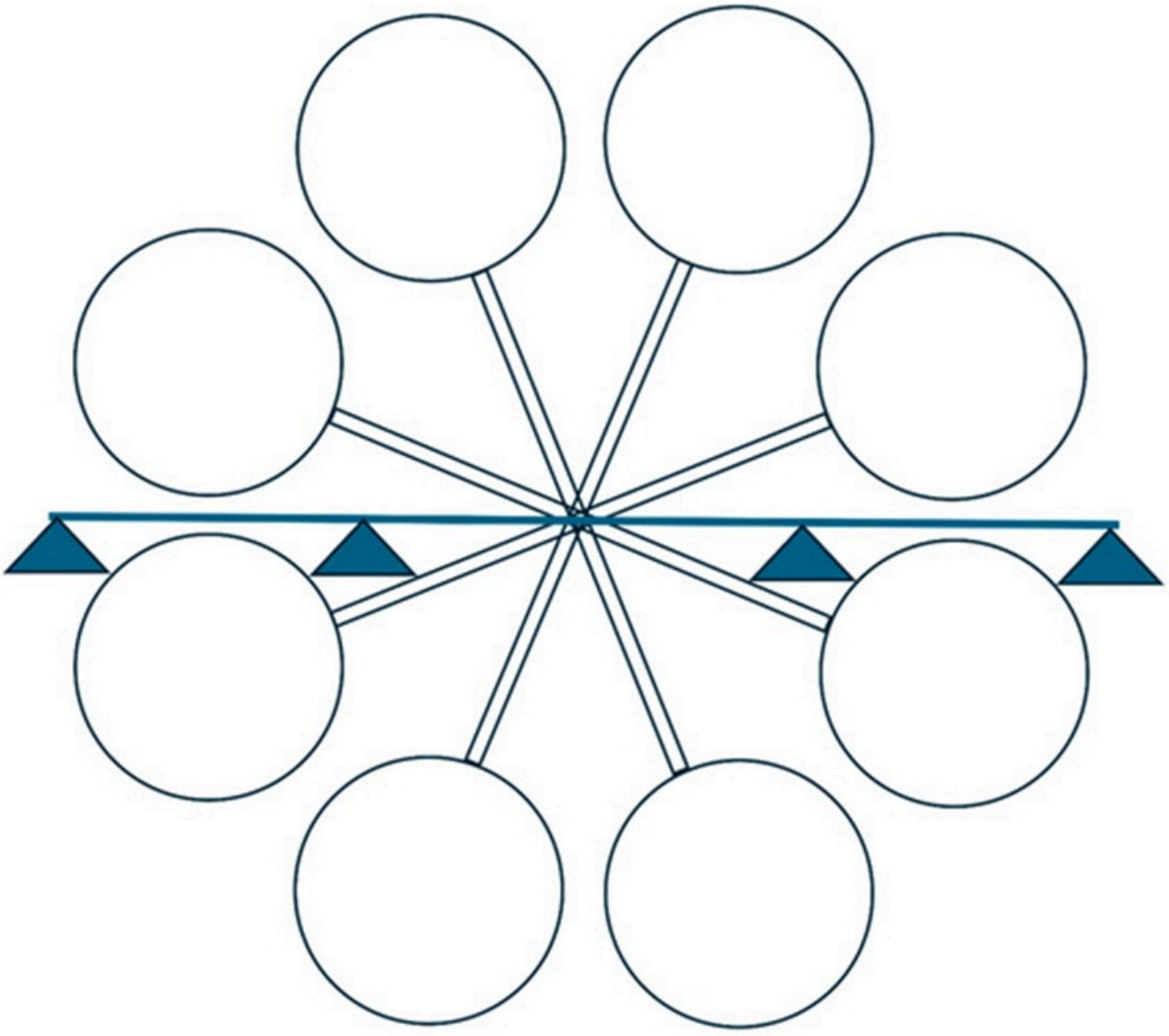

Figure 2. A schematic representation of rotor arrangement and nozzle positioning along the aircraft boom. Circular markers indicate rotor placements, while triangular markers denote the nozzles discharging simulated flat-fan spray patterns. Nozzles were situated at 18″ (45.7 cm) and 32″ (81.3 cm) from the aircraft centerline for the inboard and outboard positions, respectively.

The aircraft, carrying a tank mixture composed of tap water blended with Vision Pink™ dye (GarrCo Products, Converse, IN, USA) at a concentration of 20 mL·L−1, traversed perpendicular to the prevailing wind (± 30°) along a 30 m sampling transect **(Figure 3)**. The aircraft maintained flight at the −2.5 m waypoint, operating at an altitude of 3 m and a forward velocity of 3 m·s−1. Nozzle operating pressure was set to 165.5 kPa, the minimum required to sustain a coherent flat-fan pattern, which helps minimize drift. This reduced system pressure nonetheless yielded a lower flow output (0.46 L/min), translating into a lower volumetric application rate (4.3 to 8.6 L/ha), depending on the specific nozzle. The operational flight parameters adhered to for the V8A Pro aircraft throughout this study aligned with those described by Martin *et al.* [15].

© 2022 The Author(s). | Published by Agro Intelligence Research Press

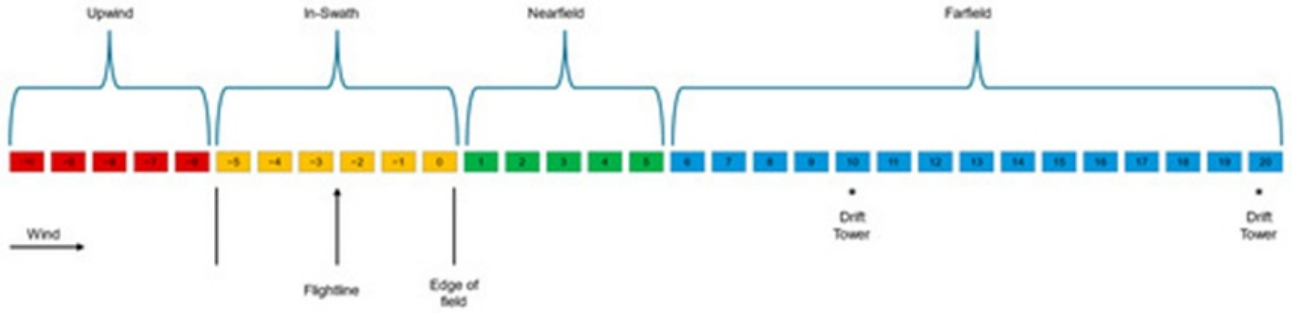

Figure 3. A sampling transect along which 31 Mylar cards were arrayed at 1 m spacing to record in-swath and downwind deposition. Drift towers.

The sampling transect was arranged parallel to the dominant wind across a caliche substrate, with ground-level collectors [Mylar cards (10 cm × 10 cm)] spaced at 1 m **(Figure 3)**. The sampling transect, dimensioned in mm, was subdivided into upwind (−10 to −6), in-swath (−5 to 0), near field (1 to 5), and far field zones (6 to 20). The spray droplets travelled along the sampling transect upon which the Mylar cards were situated, orthogonal to the aircraft's trajectory. For each replicate, spray deployments were performed with a filled tank to maintain a maximal, relatively steady downwash thrust. The Mylar cards, placed along the downwind fringe of the spray swath as an extension of the in-swath collectors, captured the off-target movement, or drift, of the spray material. Supplementing these collectors, monofilament lines, oriented parallel to the flight trajectory, were strung aloft at 2 m elevation and stationed at 10 and 20 m downwind from the plot boundary in each of the three treatments to trap airborne deposits.

Shortly after each spray pass concluded, the Mylar card (100 cm^2) and the monofilament specimens were separately sealed within a plastic bag labelled with the run identifier, treatment, and replicate number, held in a chilled container, and delivered to the analytical facility. There, 20 mL of ethanol was added to each bag, the bags were vigorously agitated, and 6 mL of the resulting supernatant was transferred to a cuvette. The cuvettes were subsequently loaded into a spectrofluorophotometer (Shimadzu, Model RF5000U, Kyoto, Japan) configured at an excitation wavelength of 453 nm with emission captured at 488 nm. The fluorescence intensity readings were back-calculated to µg of dye/cm^2. The minimum quantifiable threshold for this dye and collection technique stood at 0.00007 µg/cm^2.

Before executing the spray drift field programme, the droplet size distributions of each nozzle type were characterised by operating the V8A Pro aircraft across a sampling array of water-sensitive paper (WSP) collectors (76 mm × 26 mm) spaced 1 m apart. WSP strips were loaded into individual paper clips fastened to a wooden mounting block in advance of each spray pass. The WSP strips were retrieved from the wooden block approximately 1 min after the completion of each spray pass and stored in photonegative sleeves (Model # 35-7BXW; PrintFile® Archival Preservers, Apopka, FL, USA). They were then transported to the laboratory for computer-assisted interpretation of the droplet-stain images captured on the collectors using the DropletScan™ scanner-based analytical suite [16]. The droplet size parameters measured were Dv0.1, Dv0.5, and Dv0.9. Dv0.1 denotes the droplet diameter (µm) below which 10% of the total spray volume resides. Correspondingly, Dv0.5 and Dv0.9 indicate the droplet diameters below which 50 and 90% of the entire spray volume is contained, respectively. The Dv0.5 metric is commonly referred to as the volume median diameter (VMD). The American Society of Agricultural and Biological Engineering (ASABE) has promulgated a standardised protocol for measuring and classifying the spray quality attributes of nozzles employed in production agriculture, ASABE S572.3, the Droplet Size Classification [17]. In keeping with this standard, the droplet dimensions discharged from the nozzle orifices in this investigation fell within the fine (106–235 µm), medium (236–340 µm), coarse (341–403 µm), and extra-coarse (404–502 µm) categories.

Determination of effective swath

© 2022 The Author(s). | Published by Agro Intelligence Research Press

The functional swath width was established through validated methodologies devised for piloted aircraft by the American Society of Agricultural and Biological Engineers (ASABE) [18]. This approach relies on multiple passes (three or more), each overlapping its predecessor, to derive a composite mean spray pattern whilst disregarding any pass with a malformed or asymmetrical distribution. The aircraft, a V8 Pro configured with XR 110-01 nozzles and loaded with a fluorescent tracer solution, navigated into the wind along a 19.2 m cotton string line positioned within the trial site deployed for the drift measurements. Spray passes were repeated on 4 occasions. The cotton string corresponding to each pass was processed through a fluorometric detection apparatus [19]. Every pass was flown in a “racetrack” configuration so that the aircraft traces a continuous looping circuit while preserving the same heading. This averaged spray pattern is subsequently subjected to computer simulation over multiple reciprocal and racetrack-style passes. The methodology adopted here conformed to the standard instituted by Operation S.A.F.E (Self-Regulating Application and Flight Efficiency), endorsed by the National Agricultural Aviation Association, for the calibration of both fixed-wing and rotary-wing aircraft with respect to spray distribution and drift characterisation [20]. The digital simulation computes the coefficient of variation (CV) across a range of swath widths. The CV acts as a metric of depositional uniformity throughout the swath width and quantifies the degree of deviation from the mean deposit [21-24]. A swath width deemed satisfactory for conventional aerial applicators is one yielding a CV ≤ 25%. An elevated CV indicates greater inconsistency in the spray pattern. Nonetheless, Smith *et al.* [25] observed that a CV of 15% corresponded to a peak-to-trough deposit ratio of roughly 1.7 and proposed that a CV below about 15% constitutes an advisable benchmark for spray operations seeking to minimise excessive application. **Figure 4** illustrates that the functional swath extended from 16 to 26 ft (4.87 to 7.92 m), while maintaining acceptable CV values ≤ 15%. For this study, a functional swath of 6 m was selected, as it yielded a more expansive swath over which the fine droplets dispersed.

© 2022 The Author(s). | Published by Agro Intelligence Research Press

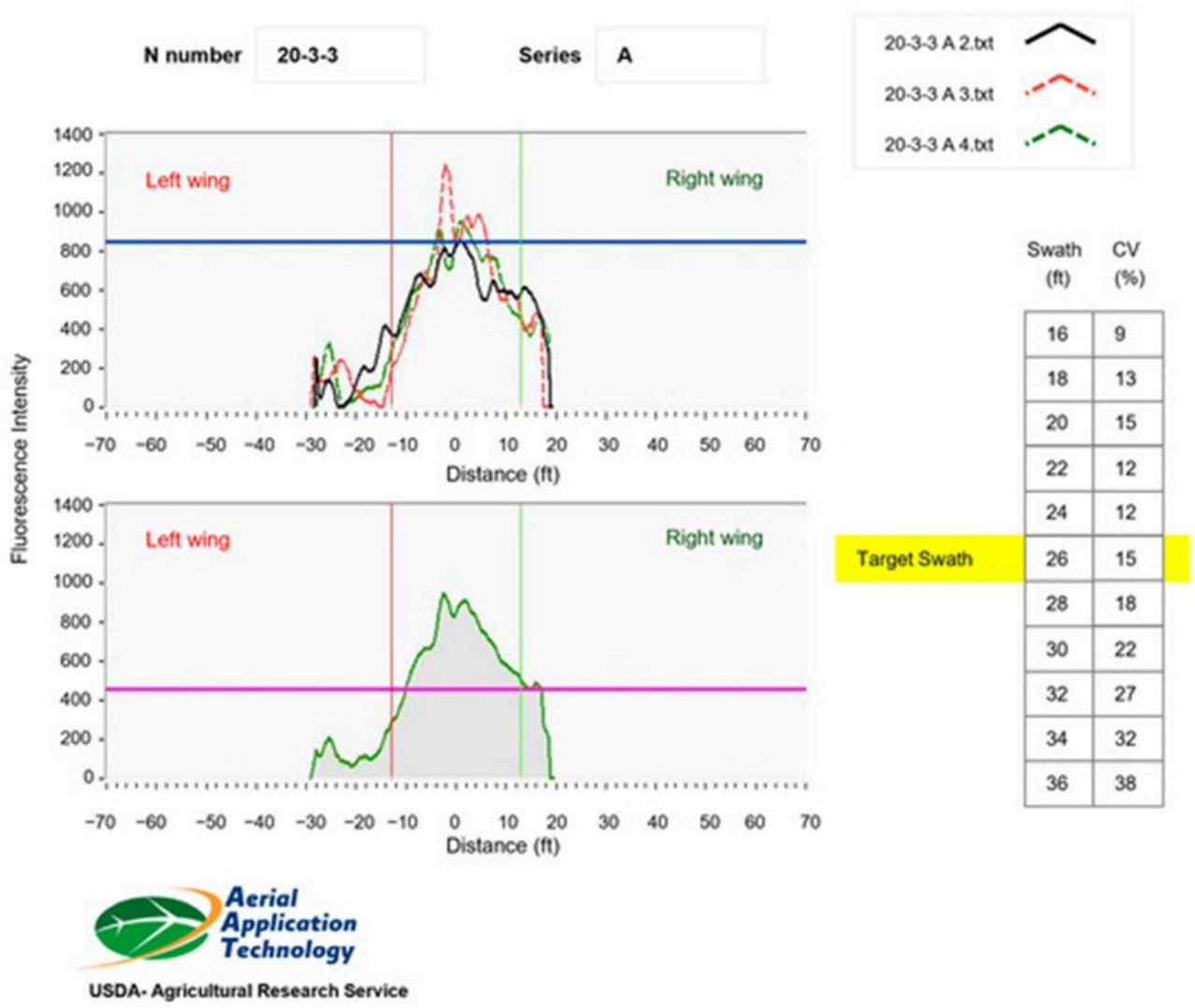

Figure 4. Determination of effective swath for the V8 Pro aircraft equipped with XR 110-01 nozzles. Three passes lapped one over the other provided an effective swath which varied from 16 to 26 ft (4.87 to 7.92 m) with acceptable CVs ≤ 15% (top graph). The average of the three passes is shown in the bottom plot. The blue and purple lines represent the target-swath average and the combined-deposit average, respectively. The vertical lines delineate the 26 ft (7.92 m) target swath width (13 ft or 3.96 m on either side of the center line).

Meteorological data

A meteorological station at Easterwood Airport, College Station, Texas, served as the source of wind velocity and direction records. These observations were logged approximately every 2 minutes. Wind direction was computed as the angular departure from parallel to the sampling transect, oriented at 143 degrees. Wind velocity was registered at a 10 m height but subsequently normalised to a 2 m equivalent through **Eq. 1**, where V_1 corresponds to the observed wind speed at the 10 m elevation (h_1), V_2 denotes the projected wind speed at 2 m (h_2), and Z_0 signifies the surface roughness coefficient [26, 27].

© 2022 The Author(s). | Published by Agro Intelligence Research Press

$$V_2 = V_1 \frac{\ln\left(\frac{h_2}{Z_0}\right)}{\ln\left(\frac{h_1}{Z_0}\right)} \quad (1)$$

For this adjustment, a surface roughness parameter of 0.03 m was assigned, characteristic of open agricultural landscapes [27], thereby accommodating the deceleration of wind flow induced by frictional drag at the terrestrial interface.

Wind records were matched to the chronometric window of each run as closely as circumstances permitted, relying on informed professional evaluation. Where a wind measurement coincided temporally with the spray run window, that solitary datum was utilised. In cases where no measurement fell within the spray run window, observations immediately preceding and succeeding the run time were scrutinised. If a pair of flanking measurements each fell within one minute of the spray run window, their mean was computed. Runs during which the wind direction strayed beyond > ± 30° from the UAV flight alignment or that exhibited 0 m/s wind velocity were discarded, culminating in a dataset of 23 runs. This practice is consistent with ASABE Standard S561.1, which addresses spray drift quantification by aerial vehicles [28]. **Table 1** confirms that the meteorological parameters recorded during this study remained stable, with no anomalous fluctuations. At the same time, **Figure 5** depicts both the wind direction and wind velocity encountered throughout the experiments chronicled herein.

© 2022 The Author(s). | Published by Agro Intelligence Research Press

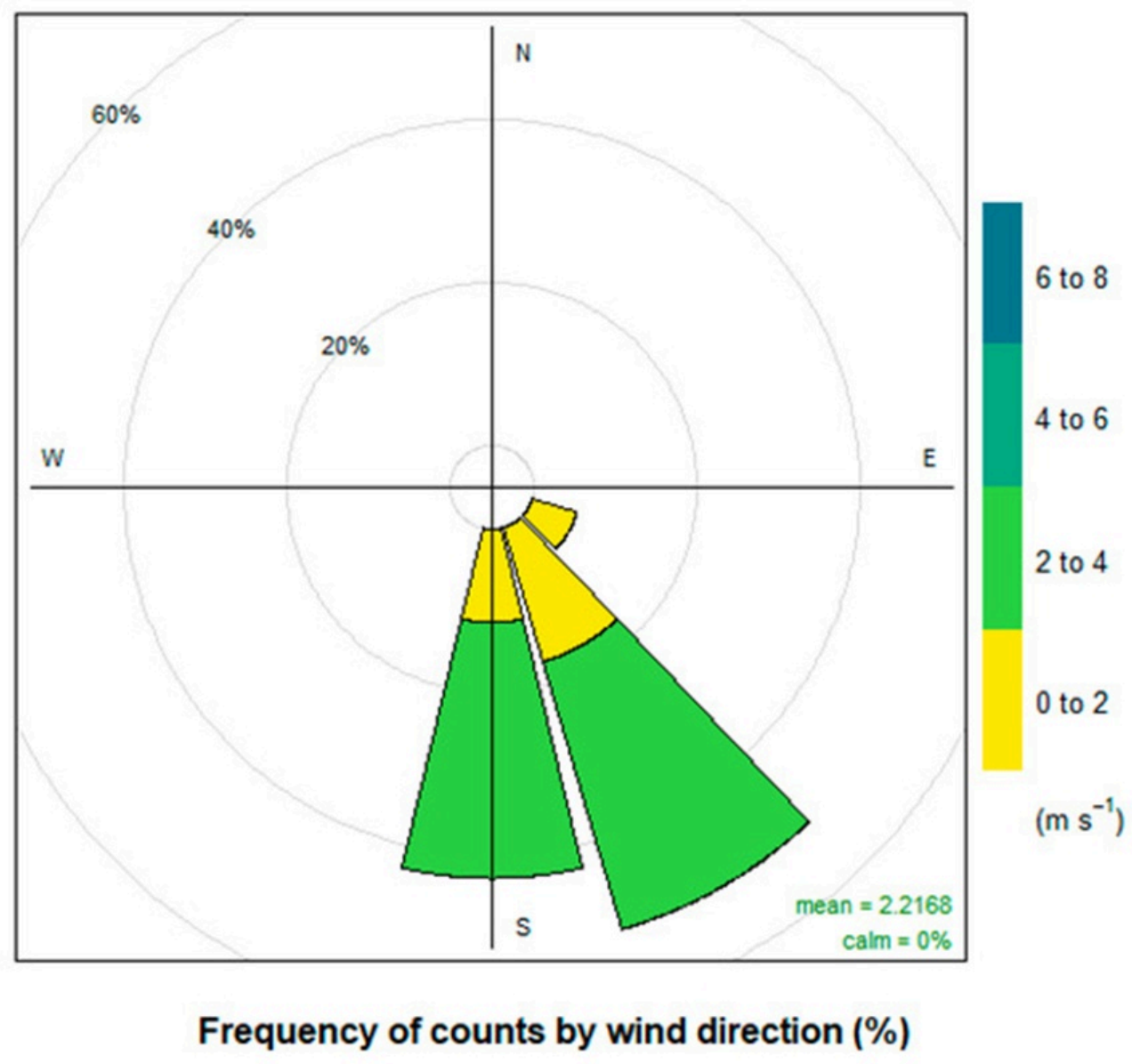

Figure 5. Wind rose showing the wind speed and predominant wind direction during the field trial.

Table 1. Meteorological data (mean ± SEM) were measured and calculated for each treatment in this study.

Treatment (Nozzle)	Temperature (°C)	Relative Humidity (%)	Wind Direction (°)	Wind Speed (2 m)	Wind Speed (10 m)
Fine	30.8 ± 0.6	71.3 ± 2.4	151.5 ± 7.4	1.51 ± 0.29	2.08 ± 0.41
Medium	30.9 ± 0.6	70.5 ± 2.4	157.0 ± 8.4	1.54 ± 0.28	2.13 ± 0.38
Extra Coarse	31.1 ± 0.6	70.0 ± 2.4	167.8 ± 9.8	1.35 ± 0.30	1.87 ± 0.42

Data analysis

Downwind deposition measurements obtained with Mylar cards served as the basis for constructing spray drift profiles and for comparative assessments across nozzle categories. Within the set of 23 runs where the documented wind

© 2022 The Author(s). | Published by Agro Intelligence Research Press

direction remained inside the <±30° envelope and wind velocity surpassed 0 m/s, the breakdown consisted of 9 fine, 8 medium, and 6 extra-coarse nozzle runs, respectively. Drift profiles were delineated spanning 1 to 20 m downwind of the drone, assuming a spray swath width of 6 m (3.0 m in each direction). Because every deposition observation registered at distances from 7.5 m outwards for the extra-coarse nozzle treatment fell beneath the < LOD (limit of deposition), these data points were removed from the model. The total corpus of observations utilised amounted to 424 (14 distances per extra-coarse nozzle run and 20 distances per each of the remaining nozzle types).

The variability inherent in deposition, expressed in μg/cm², was scrutinised through linear mixed-effects (LME) modelling following the framework articulated by Kuznetsova *et al.* [29]. To satisfy the assumptions of linearity, homoscedasticity, and residual normality, the cube root transformed deposition, while the natural logarithm transformed distance. Additional fixed-effects terms included the nozzle as a categorical predictor, wind velocity in m/s, the cosine of the wind angle relative to parallel, and the interaction term wind speed × cosine(angle), designed to encapsulate both properties simultaneously. The random effects structure specified replicate as the grouping factor to accommodate random intercepts. All statistical computations were executed within the R software environment version 4.2.0 [30], including the derivation of an $R^2\beta$ statistic [31, 32] using the standardised generalised variance methodology. At the same time, graphical outputs were generated using the data visualisation toolkit ggplot2 [33].

Variations in in-swath deposition between nozzle types were likewise examined. The deposition retained on Mylar cards situated at distances from −5 to 0 m, spanning a 5 m corridor centred upon the drone's flight line, was aggregated within each replicate. These cumulative values were stratified by nozzle category and subjected to ANOVA, followed by a Tukey post hoc test to discriminate among nozzle groups [30]. Residual diagnostics were inspected to confirm adherence to normality and variance homogeneity assumptions.

Beyond quantifying the effect of nozzle selection on drift behaviour, it remains equally vital to characterise how deposition differs among nozzles at each discrete sampling coordinate. Accordingly, the in-swath and downwind deposition datasets collected along sampling transects that showed significant interaction effects were analysed using the least-squares means function (adjust = Tukey) in the PROC GLIMMIX procedure [34]. The droplet size spectra documented before the drift trials were evaluated to establish whether each spectral metric (Dv0.1, Dv0.5, and Dv0.9) varied significantly between nozzle configurations. To stabilise the error variances, the Mylar card and monofilament line data were subjected to X + 1 and Normal Quantile transformations, respectively, before conducting ANOVA. Graphical rendering of the datasets was accomplished through the SAS/JMP® [35] software package, utilising the untransformed observations.

Results and Discussion

Droplet size classification

Spray plumes emanating from the nozzle orifices were constituted of fine, medium, and extra-coarse droplet fractions. ANOVA outputs confirmed that all three droplet spectrum indices diverged significantly across the nozzle variants tested (Dv0.1: $F = 16.68$; $P < 0.0001$; Dv0.5: $F = 18.22$; $P < 0.0001$; and Dv0.9: $F = 8.68$; $P < 0.0006$), with MSE df = 46 applying uniformly to each spectrum. **Figure 6** reveals that Dv0.1 droplets were markedly smaller for the fine and medium nozzle configurations than those released by the extra-coarse nozzle. Dv0.1 droplet dimensions were statistically indistinguishable between the fine and medium nozzles. In parallel, Dv0.5 droplets were smaller in the fine- and medium-nozzle treatments than in the extra-coarse nozzle treatment. The Dv0.9 droplets were substantially larger in the medium and extra-coarse nozzle configurations than in the fine nozzle configuration. Dv0.9 droplet sizes for the medium and extra-coarse nozzles were found to be comparable.

© 2022 The Author(s). | Published by Agro Intelligence Research Press

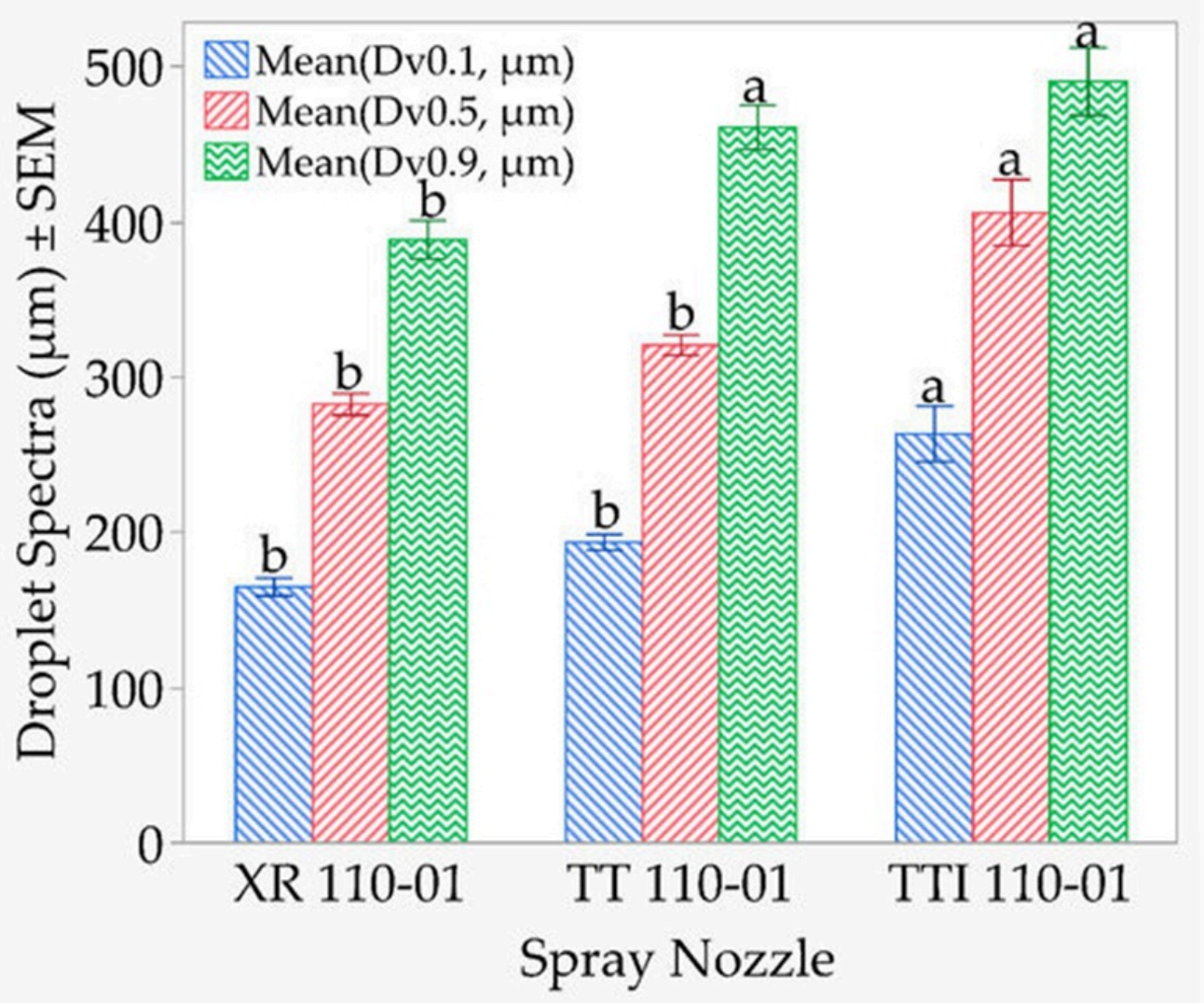

Figure 6. Spray droplet spectra of the spray nozzles (fine, medium, and extra coarse) employed in this study. The droplet images captured on WSP collectors were analysed using computer-based software. Means ± Standard Error of the Mean (SEM) among spray nozzles within each droplet spectrum, followed by the same lower-case letters, are not significantly different at α = 0.05 (Tukey's HSD test).

Deposition on mylar cards

Examination of variance across the upwind, in-swath, and near-field Mylar card deposit data yielded a significant interaction tied to sampling position ($F = 2.63$; $df = 30, 320$). Looking at **Figure 7**, one sees that at the furthest upwind point (−6 m), markedly reduced accumulation was observed with the extra-coarse nozzle; however, the disparity between the extra-coarse and fine nozzle outputs did not meet the significance criterion. What did emerge clearly was that extra-coarse nozzle deposition fell significantly short of that produced by the medium nozzle. Much the same pattern carried forward to the −5 m in-swath marker. In the in-swath zone, the extra-coarse configuration exhibited rising deposit levels, culminating at −3 m, where this nozzle type significantly outperformed both the medium and fine variants in collected quantity. This advantage in deposition for the extra-coarse treatment over the in-swath segment held until reaching −1 m, at which point the relationship flipped and extra-coarse nozzle accumulations underwent a steep, asymptotic decline. Shifting to the near-field region, the extra-coarse nozzle consistently underperformed, yielding significantly lighter deposits than either medium or fine alternatives.

© 2022 The Author(s). | Published by Agro Intelligence Research Press

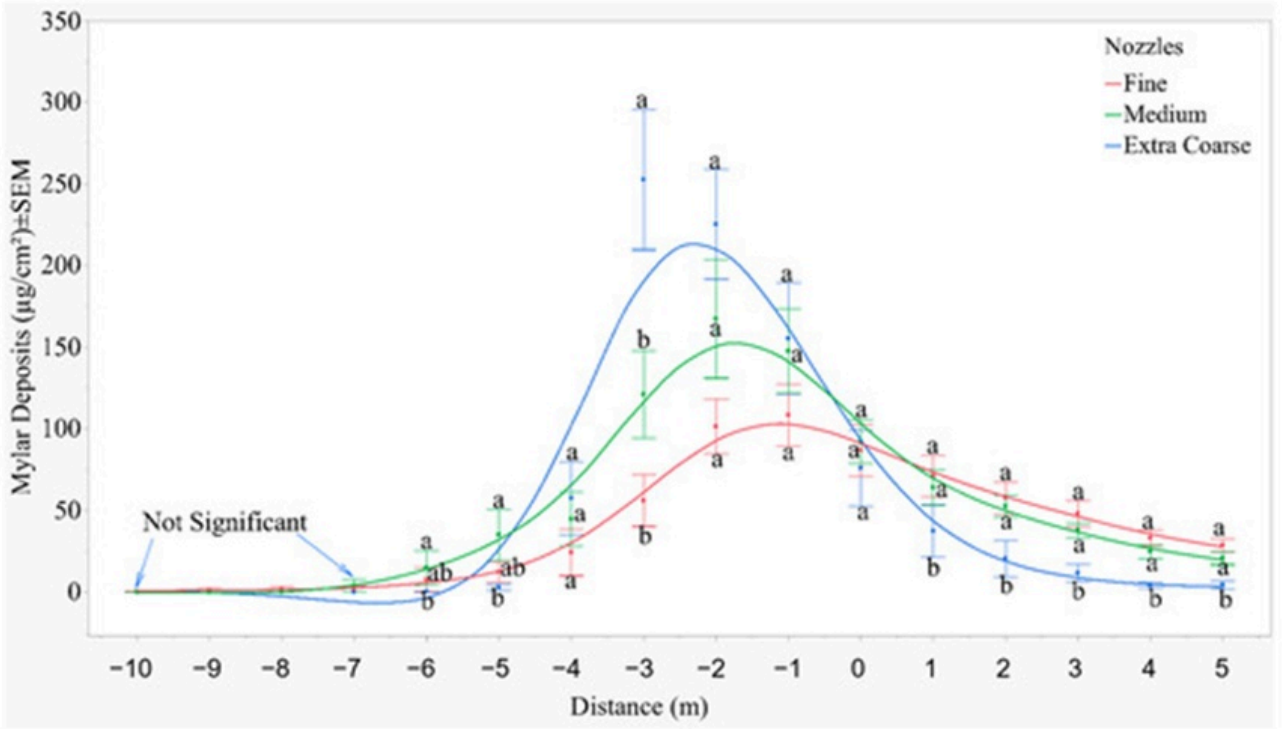

Figure 7. Spray deposition on Mylar cards. Data were analyzed using the log(x + 1) transformation, and the original means are presented here. Means ± Standard Error of the Mean (SEM) within each sampling line location with the same lower-case letters are not significantly different at α = 0.05 (Tukey's HSD test).

What **Figure 8** captures is the off-target airborne travel—drift of the spray mixture once it leaves the aircraft. Reliable treatment-level separations were evident across the span from position 6 to 17 m, during which extra-coarse nozzle drift was significantly reduced relative to the fine nozzle. Covering the band from 6 to 8 m downwind, extra-coarse deposits proved significantly sparser than those of both medium and fine nozzle classes. At the same time, the latter two could not be reliably told apart. By contrast, the 9-to-12 m downwind stretch featured clear partitioning among all three nozzle varieties. From 13 through 17 m downwind, the extra-coarse nozzle remained significantly below the fine nozzle in captured deposition. Past these distances, none of the nozzle comparisons reached the significance threshold.

© 2022 The Author(s). | Published by Agro Intelligence Research Press

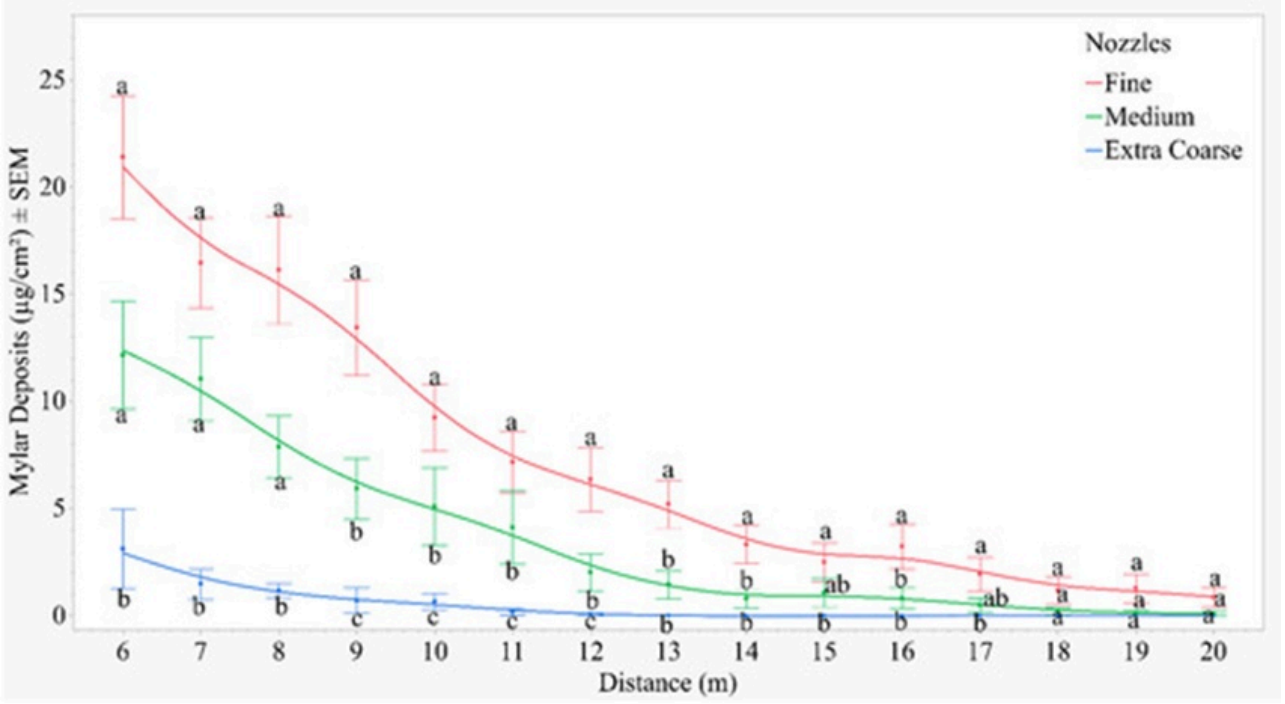

Figure 8. Downwind spray deposition on Mylar cards. Data were analyzed using the log(x + 1) transformation, and the original means are presented here. Means ± Standard Error of the Mean (SEM) within each sampling line location, followed by the same lower-case letters, are not significantly different at α = 0.05 (Tukey's HSD test).

Downwind spray deposition curves

The dispersion characteristics of spray drift downwind from the drone were formalised through LME modelling. Comprehensive model diagnostics are residual behaviour is depicted in **Figure 9**. An $R^2\beta$ of 92% was secured for the full model, with residual scatter conforming acceptably to linear and normal expectations. The fitted relationship is distilled in the predictive formula below, suited to approximating mean deposition under combinations of distance, wind speed, and nozzle selection **(Eq. 2)**.

$$\text{Deposition} = (4.94 - 1.28\ln(\text{Dist}) + 0.82W - 0.36N_M - 1.31N_C - 0.30[\ln(\text{Dist}) \times W])^3 \quad (2)$$

Where deposition is in µg/cm²; Dist = distance in m; W = wind speed in m/s; NM = a binary indicator of the medium nozzle (1 where the nozzle is medium; 0 where it is not); and NC = a binary indicator of the extra-coarse nozzle. The fine nozzle provides the reference structure and is therefore estimated by collapsing the NM and NC terms to zero.

© 2022 The Author(s). | Published by Agro Intelligence Research Press

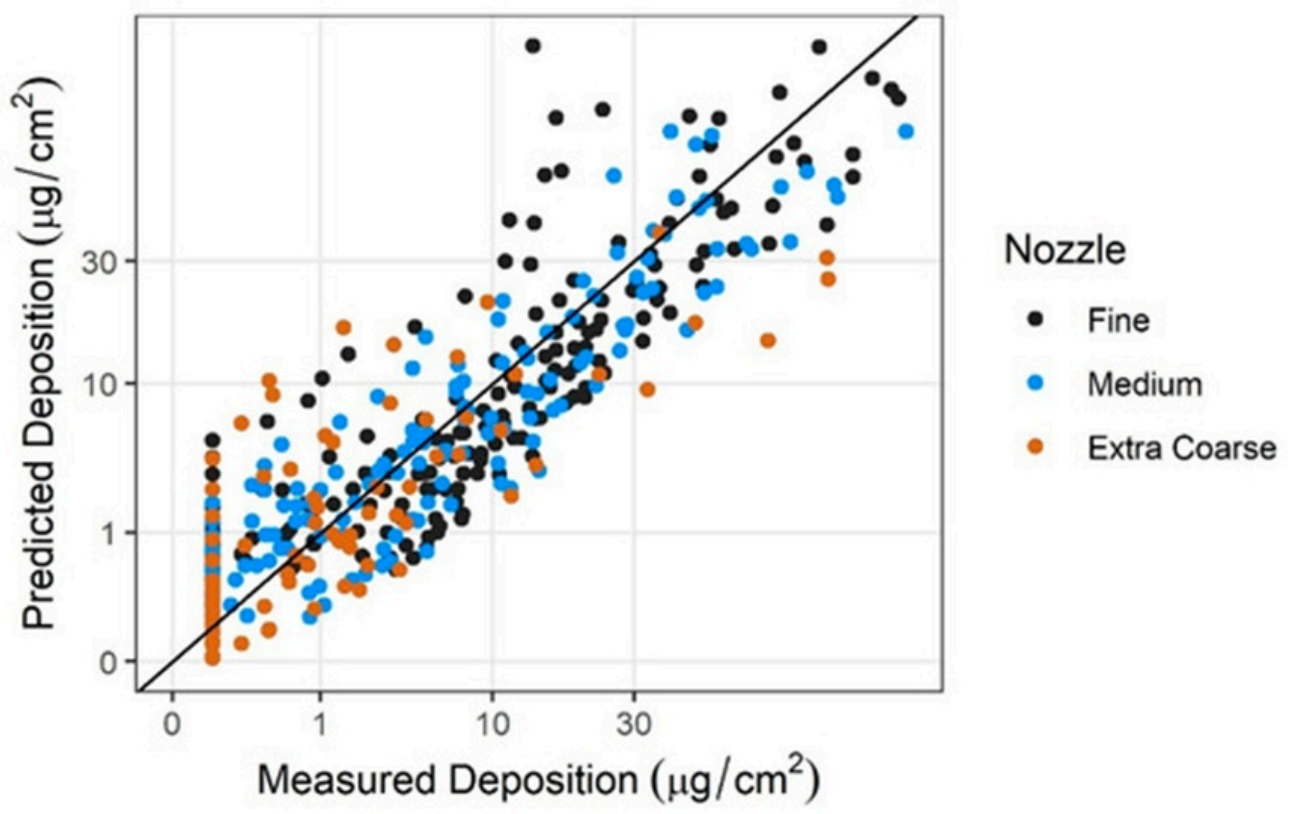

Figure 9. Graph of residual errors from the downwind spray drift deposition LME model. Points above the 1:1 line were overestimated, and those below were underestimated. Predictions were calculated without random effect shifts. Both axes are plotted on the cube-root scale, as shown.

Deposit levels associated with the extra-coarse nozzle were substantially lower than those of both competing nozzle categories (P = 0.0018 compared with medium and P = 0.0001 compared with fine, derived using the emmeans package [36]). To offer a concrete case, at the minimum downwind offset evaluated (3.5 m) and with the wind speed fixed at its overall average (2.1 m/s), deploying the extra-coarse nozzle undershot the medium-nozzle runs by an average of 34.0 µg/cm² and fell short of the fine-nozzle runs by 52.8 µg/cm². When the measurement distance was extended to 20.5 m from the drone, extra-coarse fell beneath medium by a negligible 0.2 µg/cm² and beneath fine by just 0.8 µg/cm² on average.

Although the nozzle predictor as a whole was significant (P = 0.0005), the deposit behaviour of the medium nozzle closely mirrored that of the fine nozzle (P = 0.14). Replicate variability within these two nozzle groups was considerable, producing enough distributional overlap that the computed confidence bands lacked the narrowness required to tease them apart (note the coincident shaded 95% confidence regions in **Figure 10**).

© 2022 The Author(s). | Published by Agro Intelligence Research Press

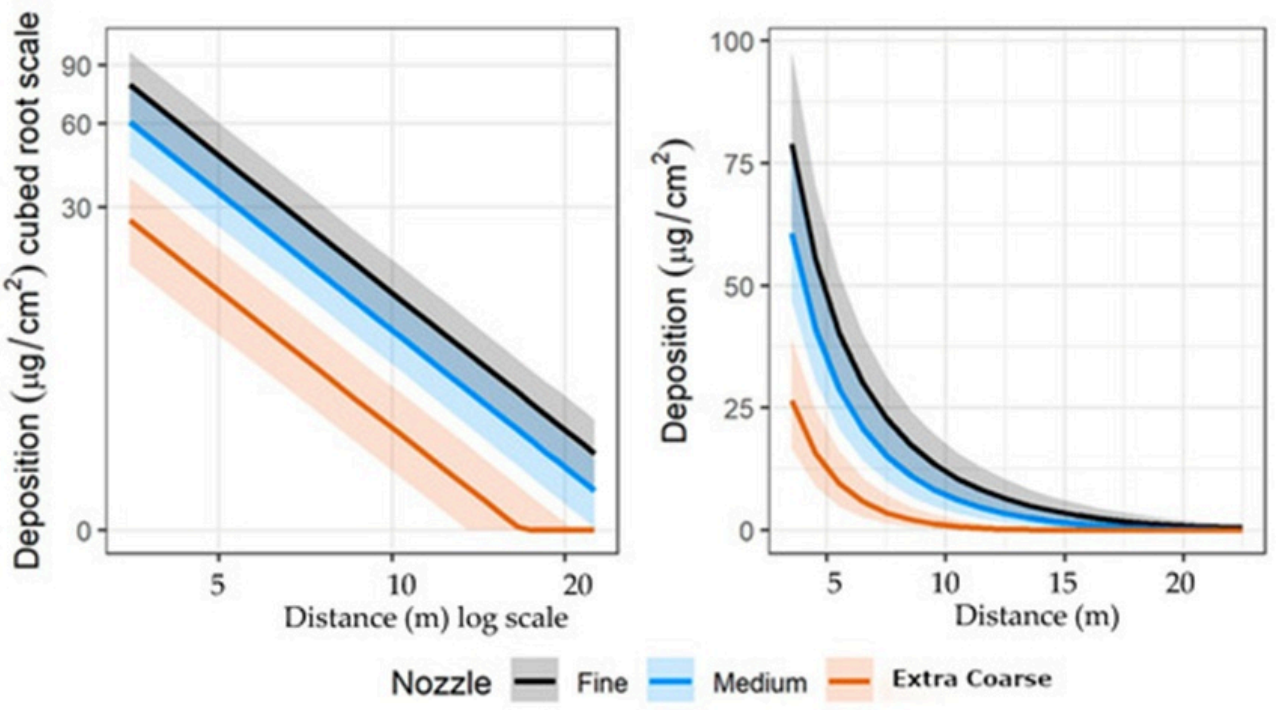

Figure 10. Downwind spray drift deposition curves for each nozzle with shaded 95% confidence intervals, shown at the mean wind speed (2.1 m/s). (Left): axes scaled as modeled; (Right): standard scale. The fine and medium nozzles are more similar in range compared to the distinctly lower extra-coarse nozzle. For 7.5 m and above, extra-coarse nozzle depositions were predicted to be nondetectable.

Swifter winds coincided with intensified deposition at sampling stations near the drone (P-value of intercept shift = 0.0004). Yet, these contrasts dissipated into non-significance as distance increased (P-value of slope shift < 0.0001). **Figure 11** visually renders the gradual erosion of the wind speed signature. Wind speed shared a correlational structure with deposition heterogeneity and partly absorbed it. Its role, therefore, was that of a covariate, tightening the estimated contrasts among nozzle means.

© 2022 The Author(s). | Published by Agro Intelligence Research Press

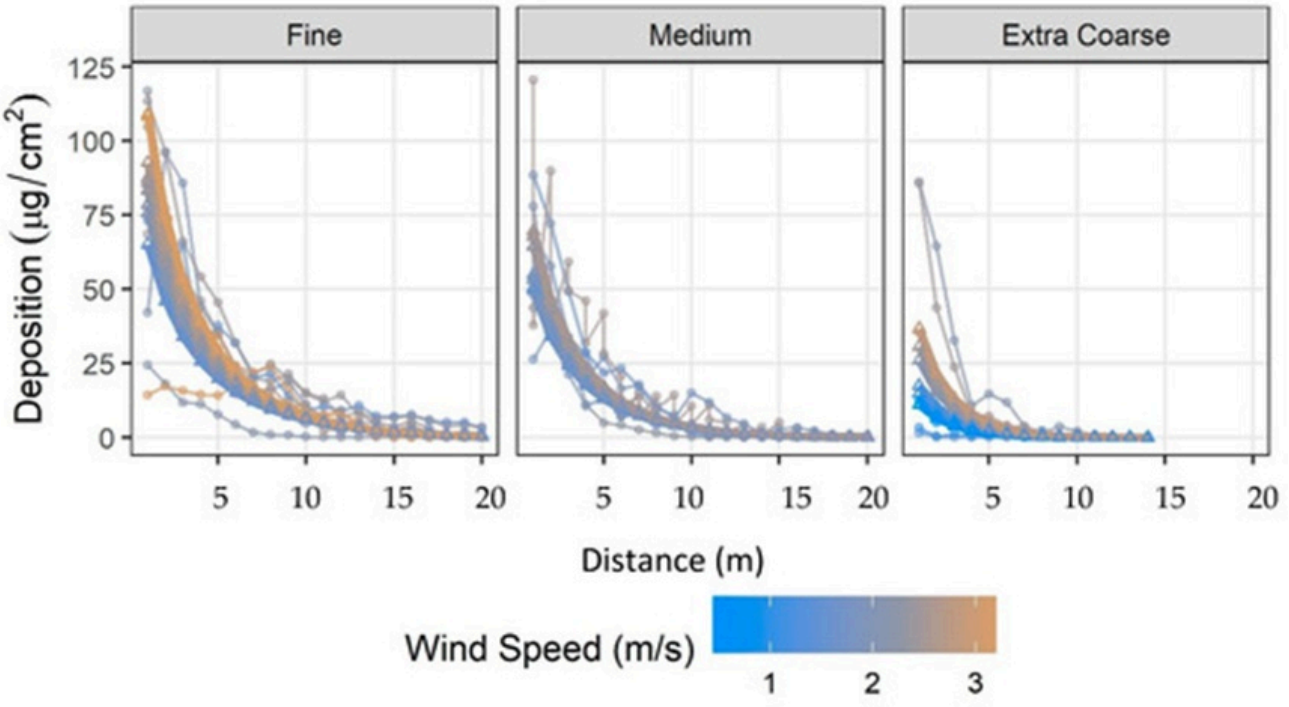

Figure 11. Actual downwind depositions (thinner lines with circle points) and predicted depositions from the LME model (thicker lines with triangles). Wind speed varied the predictions, such that faster speeds led to greater deposition at closer distances.

A single observation warrants particular mention, as the model failed to accommodate it adequately. During fine nozzle replicate 7, the 3.5 m downwind location—the closest monitored—gave an observed reading of 14.3 µg/cm², yet the model returned a fitted estimate of 109.0 µg/cm². The depositional contour of this specific run stood out: measurements spanning the 3.5-to-9.5 m interval formed an almost level plateau rather than tracing the expected downward slope. The run in question coincided with the upper limit of wind speed in the analytical dataset (3.2 m/s); outside this range, no additional evidence emerged to rationalise its anomalous signature.

Deposition on monofilament lines

The spray fraction captured on monofilament lines—representing the component most vulnerable to off-target movement—is shown in **Figure 12**. Variance partitioning confirmed that both nozzle type ($F = 29.78$; $P < 0.0001$; $df = 2, 113$) and collector position operated as highly consequential sources of variation ($F = 22.89$; $P < 0.01$; $df = 1, 113$), while their joint effect fell short of significance ($F = 2.70$; $P > 0.0.07$; $df = 2, 113$). As the downwind displacement of the sampling station increased, the collected deposit diminished steeply. In both the fine and medium configurations, the extra-coarse nozzle produced lighter airborne accumulations at both 10 and 20 m. The fine nozzle registered the highest airborne readings at 10 m. That same general pattern persisted at the 20 m station for the fine nozzle, though its values there were not statistically distinguishable from those of the medium nozzle. Pooling all records, mean monofilament line depositions stood at 14.80 ± 1.77, 5.51 ± 1.16, and 0.37 ± 0.12 µg/cm² for the fine, medium, and extra-coarse treatments, respectively, with each contrast attaining significance **(Figure 13)**.

© 2022 The Author(s). | Published by Agro Intelligence Research Press

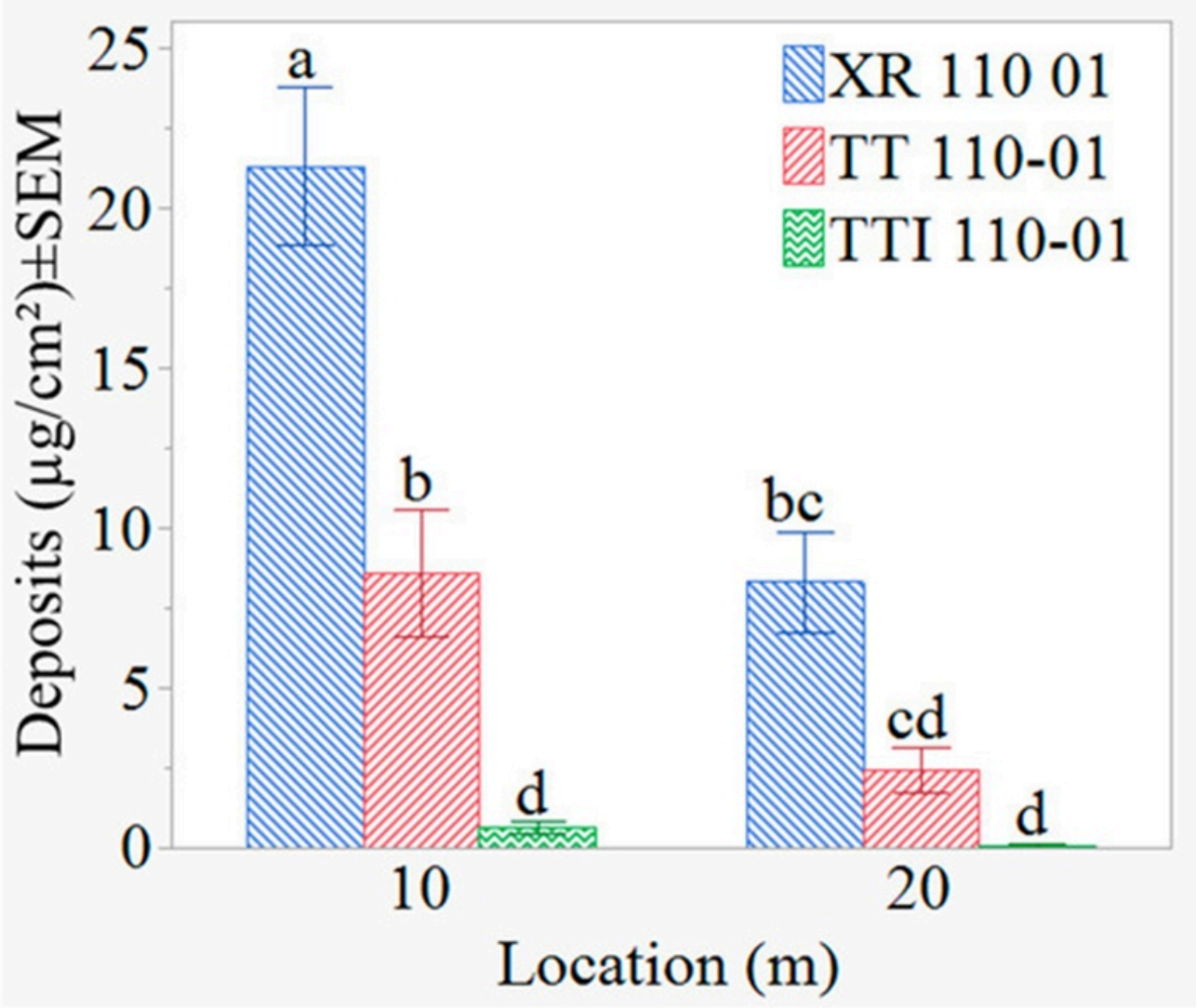

Figure 12. Deposition on monofilament lines at 10 and 20 m distances downwind. Means ± Standard Error of the Mean (SEM) with the same lower-case letters are not significantly different at α = 0.05 (Tukey's HSD test). The data were analyzed using the Normal Quantile transformation, but the results are presented as original means.

© 2022 The Author(s). | Published by Agro Intelligence Research Press

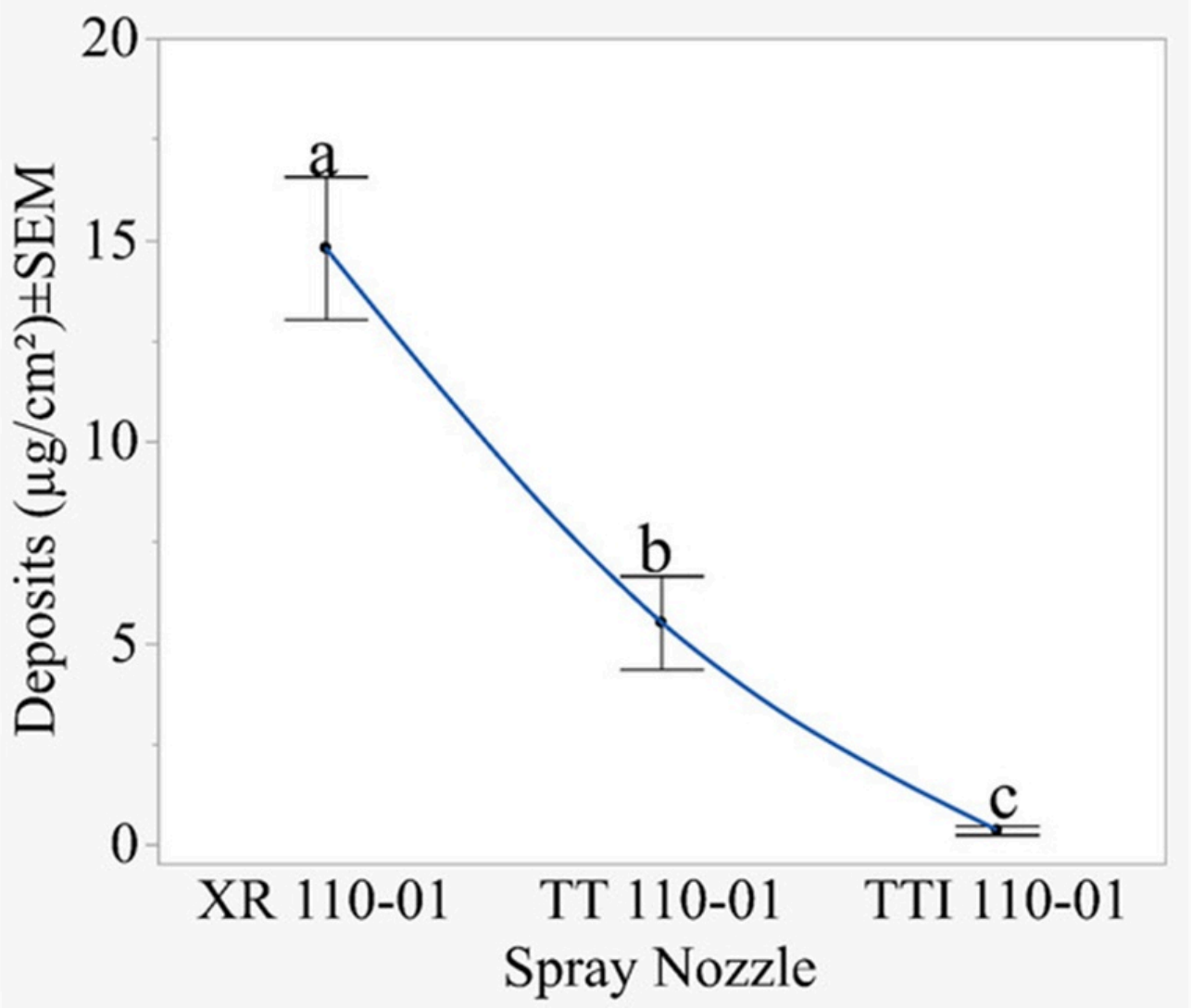

Figure 13. Overall spray deposits on monofilament lines established for the fine, medium, and extra-coarse nozzle treatments. Means ± Standard Error of the Mean (SEM) followed by the same lower-case letters are not significantly different (HSD test) at P = 0.05. The data were analyzed using the Normal Quantile transformation, but the results are presented as original means.

The scholarly literature has long held that pesticide drift originates chiefly from fine spray fractions, whereas the extra-coarse output typical of air-induction designs proves considerably less susceptible to off-target movement. What the current findings confirm is a clear inverse relationship: enlarging droplet dimensions corresponded directly to a contraction in downwind particle travel. Among the nozzles trialled, the TTI 110-01—a flat-fan, air-induction model discharging extra-coarse droplets—left the scantiest residue on Mylar surfaces positioned beyond the treatment swath. This outcome harmonises with the work of Wang *et al.* [37], whose wind tunnel evaluation of UAV drift potential concluded that air-induction configurations outperformed both hollow-cone and flat-fan alternatives in drift reduction. A parallel story emerged from the monofilament line data collected at the two drift tower distances: airborne catch was significantly leaner for the air-induction treatment than for either the fine or medium cohort. The centrality of droplet calibre—and hence nozzle choice—to drift behaviour cannot be overstated. Fine, diminutive, readily aerosolised droplets are swept along air currents, whereas their extra-coarse counterparts, despite being drift-capable, tend to settle out immediately beneath the platform. The physics are straightforward: coarser droplets, being more massive, maintain a downward velocity for a longer period before contacting the target, thereby limiting their horizontal excursion.

© 2022 The Author(s). | Published by Agro Intelligence Research Press

A further insight from this study is confirmation that wind speed is an indispensable covariate in shaping droplet flight paths. A potentially confounding circumstance warrants mention: the lowest wind velocities on record coincided with the test intervals during which the extra-coarse nozzle was fitted. To probe whether this temporal alignment might have biased the drift estimates, the LME model was recomputed with those two runs omitted. The revised output showed the wind speed intercept slipping to non-significance (P = 0.113), whilst the negative slope component held its significance (P = 0.026)—a pattern suggesting that, although the overall explanatory weight carried by wind speed diminished somewhat, the direction of its effect remained intact. Concurrently, the coefficient attached to the extra-coarse nozzle underwent a slight upward adjustment (shifting from −1.31 to 1.27) yet preserved its statistical significance, thereby affirming that these particular observations did not unduly shape the core conclusions. Such modelling exercises illustrate the value of analytical frameworks capable of isolating covariate effects, such as wind speed, providing a scaffold upon which mechanistic understanding and forward prediction of drift under heterogeneous field conditions can be progressively refined, all while functioning as an adjunct to direct empirical measurement.

The role of rotor-generated airflow has been addressed by Teske *et al.* [38], who proposed that UAV downwash can actively propel spray material groundward when the platform operates within an optimal speed envelope. At modest forward velocities, the substantial descending air column beneath the rotors is thought to accelerate droplet sedimentation and enhance on-target pattern uniformity. At higher traverse rates, by contrast, the disturbed airflow may erode this downwash effect, thereby abetting the lateral escape of spray constituents. The present experiment, flown at a ground speed considered favourable, likely benefited from propulsive assistance by the rotors in shepherding the tank mix toward its intended destination—an outcome consistent with the study's original objectives. Hunter *et al.* [39] have separately highlighted the role of release height, noting that higher operational altitudes expose the droplet plume to wind regimes capable of ferrying entrainable material beyond the designated zone, a risk mitigated by the comparatively low release height maintained here.

Adopting a simulation-based perspective, Yang *et al.* [40] characterised the post-nozzle journey of a spray droplet as a contest between the horizontal and vertical force fields generated by the UAV. Teske *et al.* [38] emphasised the practical importance of identifying the ground speed at which rotor downwash degrades into lateral outwash before the spray reaches the crop canopy. As traverse speeds increase, the compounding effect of crosswind interactions is expected to worsen off-target displacement. More broadly, atmospheric stability class and the ambient wind field arguably represent the most consequential external variables governing droplet drift.

A methodological caveat qualifying this work concerns the sourcing of wind data from an off-site meteorological station rather than from dedicated in situ instrumentation. An unavoidable degree of temporal mismatch thus clouds the wind assignments tied to individual spray runs. The liability of both wind speed and direction on sub-minute timescales makes it highly probable that some portion of the runs were paired with wind records that poorly approximated the actual conditions prevailing at the moment of application. Any future move toward stronger reliance on model-based inference from field datasets would demand substantially upgraded, co-located atmospheric monitoring.

Conclusion

The remarkable ascendance of remotely piloted aerial application systems in commercial agriculture over recent seasons has prompted an urgent call from end users for operational protocols that enable the deployment of crop protection chemistry with the least achievable drift. A robust body of evidence already attests that nozzle specification is the pre-eminent lever governing downwind deposition of the driftable component. In light of this, the present experiment was designed to quantify how three nozzle classes—spanning fine, medium, and extra-coarse droplet spectra—influence both in-swath retention and downwind escape. Airborne drift was captured on monofilament arrays extending 20 m downwind from the field margin. The droplet size envelopes released from the tested orifices fell within the ASABE bands of fine (106–235 µm), medium (236–340 µm), coarse (341–403 µm), and extra-coarse (404–502 µm). The weight of evidence indicates that the extra-coarse treatment was consistently associated with attenuated surface deposits downwind and

© 2022 The Author(s). | Published by Agro Intelligence Research Press

diminished airborne concentrations relative to the medium and fine benchmarks. Wind speed was entered into the analysis as a covariate, sharpening the resolution of inter-nozzle contrasts. The data further indicate that fine, readily driftable droplets are predisposed to travel downwind on air currents. In contrast, very large, extra-coarse droplets have a propensity to descend almost vertically beneath the aircraft. Remote pilots engaged in aerial application may incorporate this nozzle technology as a foundational best management practice for drift mitigation.

Acknowledgements

The authors would like to thank Richard Crosby with Coastal Sprays for providing and piloting the RPAAS. In addition, the authors would like to thank Cory Southam with Hawks Agro and Gray Turnage and Logan Renz from Mississippi State University for their valuable assistance in conducting the field study.

Conflict of interest

During the study period, Jeffery W. Perine, Shanique Grant, and Jerri Lynn Henry were employees of Syngenta Crop Protection, LLC, and Farah Abi-Akar was an employee of Waterborne Environmental, Inc. This study received funding from Syngenta Crop Protection, LLC. The authors declare no additional conflicts of interest beyond these employment relationships and roles in the study. The authors declare that the research was conducted in the absence of any commercial or financial relationships that could be construed as a potential conflict of interest. The use of trade, firm, or corporation names in this publication is for the information and convenience of the reader. Such use does not constitute an official endorsement or approval by the United States Department of Agriculture or the Agricultural Research Service of any product or service to the exclusion of others that may be suitable.

Financial support

Syngenta Crop Protection LLC, grant number 58-3091-9-015, funded this research.

Ethics statement

None

Received: 25 Sep 2021 Revised: 29 Nov 2021 Accepted: 16 Dec 2021
Published online: 25 May 2022

Rights and permissions

Open Access The author(s) retain copyright. This article is licensed under the Creative Commons Attribution-NonCommercial-ShareAlike 4.0 International License. It may be shared and adapted for non-commercial purposes with appropriate attribution, an indication of changes, and distribution of adaptations under the same license. Third-party material may be subject to separate terms identified in its credit line. View the license at https://creativecommons.org/licenses/by-nc-sa/4.0/.

References

1. Zanelli EB, Bödecker H. Drone Market Report 2023–2030; Drone Industry Insights. 2023. https://dronelli.com/product/drone-market-report (accessed on 4 June 2024).

2. Howe S. What's Driving Growth in the Crop Spraying Drone Market?. https://www.commercialuavnews.com/europe/what-s-driving-growth-in-the-crop-spraying-drone-market#:~:text=The%20Research%20and%20Markets%20report,spraying%20drones.%E2%80%9D%20Moreover%2C%20the (accessed on 25 June 2024).

3. Jenkins D, Vasigh B. The Economic Impact of Unmanned Aircraft Systems Integration in the United States; Association for Unmanned Vehicle Systems International (AUVSI): Arlington, VA, USA, 2013.

4. Goldman Sachs Research. Drones: Reporting for Work. https://www.theverge.com/sponsored/goldman-sachs-drones/mobile (accessed on 25 April 2022).

5. Australian Pesticides and Veterinary Medicines Authority (APVMA). State of the Knowledge Literature Review on Unmanned Aerial Spray Systems in Agriculture; Australian Government: Canberra, Australia; 2021. p. 34.

6. Chen H, Lan Y, Fritz BK, Hoffmann WC, Liu S. Review of agricultural spraying technologies for plant protection using unmanned aerial vehicle (UAV). Int J Agric Biol Eng. 2021;14:38–49.

7. Organisation for Economic Co-operation and Development (OECD). Report on the State of the Knowledge—Literature Review on Unmanned Aerial Spray Systems in Agriculture; OECD Publishing: Paris, France, 2021.

8. Chen P, Douzals JP, Lan Y, Cotteux E, Delpuech X, Pouxviel G, et al. Characteristics of unmanned aerial spraying systems and related spray drift: A review. Front Plant Sci. 2022;13:870956.

9. Wang G, Han Y, Li X, Andaloro J, Chen P, Hoffmann WC, et al. Field evaluation of spray drift and environmental impact using an agricultural unmanned aerial vehicle (UAV) sprayer. Sci Total Environ. 2020;737:139793.

10. Koo D, Gonçalves CG, Askew SD. Agricultural spray drone deposition, Part 2: Operational height and nozzle influence pattern uniformity, drift, and weed control. Weed Sci. 2024;72:824–32.

11. Wongsuk S, Zhu Z, Zheng A, Qi P, Li Y, Huang Z, et al. Assessing the potential spray drift of a six-rotor unmanned aerial vehicle sprayer using a test bench and airborne drift collectors under low wind velocities: Impact of atomization characteristics and application parameters. Pest Manag Sci. 2024;80:6053–67.

12. Teske ME, Bird SL, Esterly DM, Curbisiley TB, Ray SL, Perry SG. AgDRIFT: A model for estimating near-field spray drift from aerial applications. Environ Toxicol Chem. 2002;21:659–71.

13. Martin DE, Latheef MA. Payload capacities of remotely piloted aerial application systems affect spray pattern and effective swath. Drones. 2022;6:205.

14. Fritz BK, Hoffmann WC, Wolf RE, Bretthauer S, Bagley WE, Bernards ML. Wind tunnel and field evaluation of drift from aerial spray applications with multiple spray formulations. In: Pesticide Formulation and Delivery Systems: 32nd Volume, Innovating Legacy Products for New Uses; Devisetty B, Ed.; ASTM International: West Conshohocken, PA, USA, 2013; 32: 96–113.

15. Martin DE, Woldt WE, Latheef MA. Effect of application height and ground speed on spray pattern and droplet spectra from remotely piloted aerial application systems. Drones. 2019;3:83.

16. Whitney RW, Gardisser DR. DropletScan Operator Manual; WRK of Oklahoma and WRK of Arkansas: Stillwater, OK, USA; Fort Smith, AR, USA, 2003.

17. ASABE. Spray Nozzle Classification by Droplet Spectra. In ANSI/ASAE S572.3 (FEB2020); ASABE: St. Joseph, MI, USA, 2020.

18. American Society of Agricultural and Biological Engineers (ASABE). Calibration and Distribution Pattern Testing of Agricultural Aerial Application Equipment; ASABE: St. Joseph, MI, USA, 2013; ASAE S386.2.

© 2022 The Author(s). | Published by Agro Intelligence Research Press

19. Fritz BK, Hoffmann WC, Jank P. A fluorescent tracer method for evaluating spray transport and fate of field and laboratory spray applications. J ASTM Int. 2011;8:JAI103619.

20. Gardisser DR. Operation S.A.F.E. for Quality Performance/Web Based Decision Making. 2010. https://tpsalliance.org/pdf/topics/5A-Gardisser-OperationSAFE-2010.pdf (accessed on 10 February 2024).

21. Carpenter TG, Reichard DL, Khan AS. Spray deposition from a row-crop airblast sprayer. Trans ASAE. 1983;26:338–42.

22. Grift TE, Walker JT, Gardisser DR. Spread Pattern Analysis Tool (SPAT): II. Examples of aircraft pattern analysis. Trans ASAE. 2000;43:1351–62.

23. Yates WE. Spray pattern analysis and evaluation of deposits from agricultural aircraft. Trans ASAE. 1962;5:49–0053.

24. Whitney RW, Kuhlman DK. Pattern analysis of agricultural aircraft. SAE Trans. 1983;92:169–77. https://www.jstor.org/stable/44647596 (accessed on 26 March 2024).

25. Smith DB, Oakley D, Williams E, Kirkpatrick A. Broadcast spray deposits from fan nozzles. Appl Eng Agric. 2000;16:109–13.

26. Justus CG, Mikhail A. Height variation of wind speed and wind distribution statistics. Geophys Res Lett. 1976;3:261–4.

27. Ragheb M. Wind Shear Roughness Classes and Turbine Energy Production. http://www.ragheb.co/NPRE%20475%20Wind%20Power%20Systems/Wind%20Shear%20Roughness%20Classes%20and%20Turbine%20Energy%20Production.pdf (accessed on 10 June 2021).

28. ASABE. ASAE Standard S561.1: Procedure for Measuring Drift Deposits from Ground, Orchard, and Aerial Sprayers; American Society of Agricultural and Biological Engineers (ASABE): St. Joseph, MI, USA, 2005.

29. Kuznetsova A, Brockhoff PB, Christensen RHB. lmerTest package: Tests in linear mixed effects models. J Stat Softw. 2017;82:26.

30. R Core Team. R: A Language and Environment for Statistical Computing; Version 4.2.0; R Foundation for Statistical Computing: Vienna, Austria, 2022.

31. Jaeger B. r2glmm: Computes R Squared for Mixed (Multilevel) Models. R Package Version 0.1. 2017. https://CRAN.R-project.org/package=r2glmm (accessed on 20 June 2021).

32. Edwards LJ, Muller KE, Wolfinger RD, Qaqish BF, Schabenberger O. An R^2 statistic for fixed effects in the linear mixed model. Stat Med. 2008;27:6137–57.

33. Wickham H. ggplot2: Elegant Graphics for Data Analysis; Springer: New York, NY, USA, 2016. https://ggplot2.tidyverse.org (accessed on 20 June 2021).

34. SAS Institute Inc. SAS® Software 9.4; SAS Institute Inc.: Cary, NC, USA, 2013.

35. SAS Institute Inc. SAS/JMP®; Version 16; SAS Institute Inc.: Cary, NC, USA, 2023.

36. Lenth R. Emmeans: Estimated Marginal Means, Aka Least-Squares Means. R Package Version 1.10.6-090003. 2025. https://rvlenth.github.io/emmeans/ (accessed on 20 June 2021).

37. Wang CL, Zeng AJ, He XK, Song JL, Herbst A, Gao W. Spray drift characteristics test of unmanned aerial vehicle spray unit under wind tunnel conditions. Int J Agric Biol Eng. 2020;13:13–21.

38. Teske ME, Wachspress DA, Thistle HW. Prediction of aerial spray release from UAVs. Trans ASABE. 2018;61:909–18.

© 2022 The Author(s). | Published by Agro Intelligence Research Press

39. Hunter JE, Gannon TW, Richardson RJ, Yelverton FH, Leon RG. Coverage and drift potential associated with nozzle and speed selection for herbicide applications using an unmanned aerial sprayer. Weed Technol. 2020;34:235–40.

40. Yang F, Xue X, Cai C, Sun Z, Zhou Q. Numerical simulation and analysis on spray drift movement of multirotor plant protection unmanned aerial vehicle. Energies. 2018;11:2399.

© 2022 The Author(s). | Published by Agro Intelligence Research Press